CHEMISTRY OF MATERIALS

Article

pubs.acs.org/cm

Atomic Layer Deposition of Ga_2O_3 Films Using Trimethylgallium and Ozone

David J. Comstock and Jeffrey W. Elam*

Energy Systems Division, Argonne National Laboratory, 9700 South Cass Avenue, Argonne, Illinois 60439, United States

ABSTRACT: In this manuscript, we demonstrate a new process for the atomic layer deposition (ALD) of gallium oxide (Ga_2O_3) thin films using trimethylgallium (TMGa) and ozone. We evaluated a variety of oxygen sources for Ga_2O_3 ALD using TMGa but found that only ozone was effective. We explored the mechanism for Ga_2O_3 ALD using in situ quartz crystal microbalance, Fourier transform infrared spectroscopy, and quadrupole mass spectrometry studies. We found that TMGa dissociatively adsorbs onto the Ga_2O_3 surface to form $Ga(CH_3)_2$ surface species and liberate ~20% of the methyl ligands as CH_4. Next, the ozone reacts with these methyl species to form hydroxyl and formate surface groups and liberate CH_2O. We prepared ALD Ga_2O_3 films on Si(100) and fused SiO_2 substrates and analyzed the films using a variety of techniques. We found the Ga_2O_3 growth to be self-limiting with a growth rate of ~0.52 Å/cycle between 200 and 375 °C. Moreover, the Ga_2O_3 films were stoichiometric, free of residual carbon, and exhibited properties similar to bulk Ga_2O_3. Scanning electron microscopy revealed smooth films with good step coverage over trench structures, and X-ray diffraction showed that the films were amorphous as-deposited but crystallized to β-Ga_2O_3 upon annealing at 900 °C.

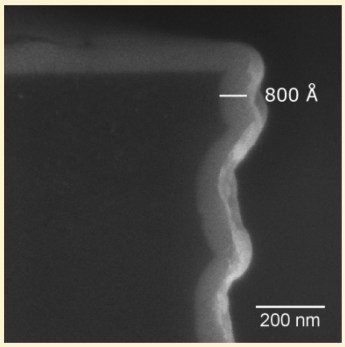

KEYWORDS: *gallium oxide, atomic layer deposition, trimethylgallium, ozone, FTIR, quartz crystal microbalance*

INTRODUCTION

Gallium oxide (Ga_2O_3) thin films have been utilized in a wide variety of applications, including phosphors,[1−4] transparent conducting oxides (TCOs),[5,6] gas sensors,[7−9] and passivating dielectrics for GaAs-based electronics.[10−12] With such varied applications, a number of techniques have been developed for depositing Ga_2O_3 thin films, including evaporation,[13,14] sputtering,[13,15] pulsed laser deposition,[5,6] chemical vapor deposition (CVD),[16−18] and atomic layer deposition (ALD).[19−24] In particular, ALD provides a number of advantages for preparing Ga_2O_3 films. ALD utilizes iterative, self-saturating precursor exposures to deposit thin films in a well-controlled, monolayer-by-monolayer fashion. As a result, ALD enables precise thickness control, high uniformity in both thickness and composition over large areas, and excellent step coverage. Furthermore, ALD is typically conducted at lower temperatures than CVD, thus enabling thermally sensitive substrates, such as polymers, to be coated.

One of the most important attributes for ALD precursors is high volatility.[25] This quality is particularly important for coating high aspect ratio or porous substrates and for scaling the ALD process to larger areas. Although Ga_2O_3 ALD processes have previously been demonstrated using $Ga(acac)_3$,[19,20] $((CH_3)_2GaNH_2)_3$,[21] $Ga_2(N(CH_3)_2)_6$,[22,23] and a Ga alkoxide,[24] all of these precursors must be heated to achieve an adequate vapor pressure. In contrast, trimethylgallium (TMGa) has a very high vapor pressure of 227 Torr at room temperature.[26] Additionally, TMGa is chemically similar and analogous to trimethylaluminum (TMA), which is considered a model precursor for Al_2O_3 ALD.[27] It is therefore somewhat surprising that there have been no reports using TMGa for Ga_2O_3 ALD, although TMGa has been utilized for Ga_2O_3 CVD at high temperatures[28] and as a dopant in the ALD of Ga-doped ZnO thin films.[29]

In this work, we demonstrate the suitability of TMGa for the ALD of high quality Ga_2O_3 films. Although a number of different oxygen sources were explored, only ozone (O_3) permitted Ga_2O_3 ALD with TMGa. We used in situ quartz crystal microbalance (QCM),[30,31] Fourier transform infrared spectroscopy (FTIR),[32−36] and quadrupole mass spectrometry (QMS)[30,37] studies to develop an understanding of the surface reactions at work during Ga_2O_3 ALD. With suitable ALD process conditions established by the in situ studies, we deposited Ga_2O_3 films on Si(100) and fused SiO_2 substrates. The properties of these films were then characterized using scanning electron microscopy (SEM), X-ray diffraction (XRD), spectroscopic ellipsometry, optical spectroscopy, Rutherford backscattering spectroscopy (RBS), and X-ray photoelectron spectroscopy (XPS).

EXPERIMENTAL SECTION

ALD was conducted in a custom, viscous flow reactor with the reaction zone consisting of a heated, 5 cm diameter, stainless steel tube.[31] The pressure within the reactor was maintained at ~1 Torr using a 300 sccm flow of ultra high purity (UHP, 99.999%) nitrogen carrier gas. Ga_2O_3 ALD was conducted using TMGa (99+%, Strem Chemicals, Inc.) as the Ga source. TMGa was dosed through a 100 μm diameter

Received: March 5, 2012
Revised: August 20, 2012
Published: October 18, 2012

   dx.doi.org/10.1021/cm300712x | *Chem. Mater.* 2012, 24, 4011−4018

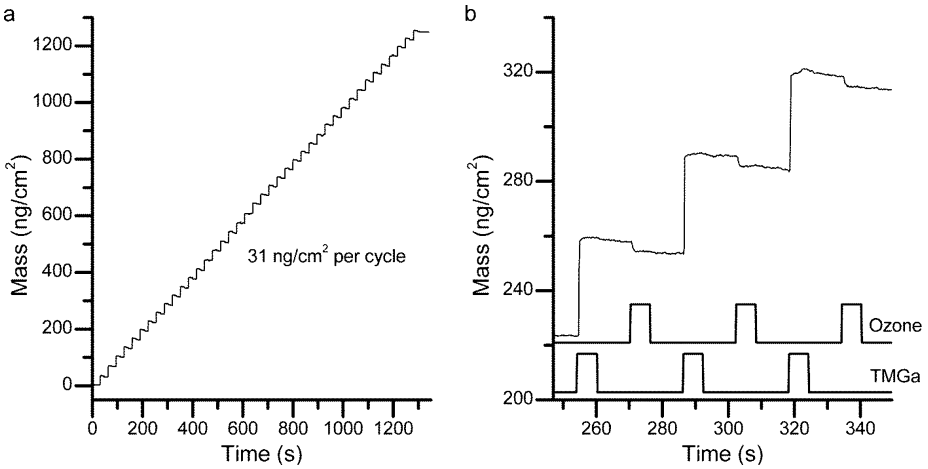

Figure 1. (a) QCM data recorded during 40 cycles of Ga_2O_3 ALD using TMGa-O_3 at 350 °C with the timing sequence 6−10−6−10. (b) Expanded view of QCM data during 3 cycles of Ga_2O_3 ALD where the individual TMGa and O_3 exposures are indicated by the lower traces.

orifice to achieve a TMGa partial pressure of ∼20 mTorr within the reactor. A variety of oxygen sources were screened, including H_2O, H_2O_2 (30 wt % in H_2O), isopropanol, O_2, O_3, and H_2O/O_2 mixtures.[38] The liquid precursor vapors (H_2O, H_2O_2, and isopropanol) were all dosed at room temperature through a needle valve. Ozone was generated by flowing UHP oxygen (99.999%) through an ozone generator (Lab-113, Pacific Ozone) at 400 sccm while keeping the pressure within the generator at 2−3 psi. The ozone generator output was approximately 8 wt % O_3 in O_2. The O_3 and O_2 were introduced into the reactor through a 200 μm diameter orifice at a backing pressure of 1 atm. The Ga_2O_3 ALD timing sequences are expressed as: t_1−t_2−t_3−t_4, where t_1 is the TMGa exposure time, t_3 is the oxygen source exposure time, and t_2 and t_4 are the respective purge times, with all times in seconds.

In situ QCM studies were conducted using a modified Maxtek Model BSH-150 sensor head loaded into the ALD reactor tube with y-12.5° cut $GaPO_4$ sensor crystals (R-20, Piezocryst Advanced Sensorics Gmbh). The y-12.5° cut $GaPO_4$ crystals are temperature compensated at 240 °C and enable QCM measurements with enhanced stability at temperatures greater than 200 °C.[39] The mass changes per unit area were calculated by measuring the frequency shifts and applying the Sauerbrey equation.[39]

In situ QMS measurements were conducted with a differentially pumped QMS (Stanford Research Systems, Model RGA300) located downstream from the sample position and separated from the reactor by a 35 μm orifice. In order to detect species with m/e ∼28, the carrier gas was changed to UHP Ar (99.999%) for these studies. Additionally, no samples were loaded into the reactor during these studies, so just the surface area of the reactor tube is responsible for the reaction products observed.

In situ FTIR studies of Ga_2O_3 ALD were conducted in transmission mode using a Nicolet 6700 FTIR spectrometer (Thermo Scientific) and a smaller reactor that is similar to those described previously.[32,40] The FTIR reactor utilized gate valves that were closed during the precursor exposures to prevent growth on the CsI windows. Substrates for FTIR measurements were prepared by pressing a nanopowder into a stainless steel grid.[41] The grids were fabricated using photochemical machining (Fotofab, Inc.) and were 50 μm thick with 50 μm bars and 200 μm square openings. Depending upon the FTIR features of interest, either ZrO_2 (<100 nm diameter) or SiO_2 (10−20 nm diameter) nanopowders were utilized. ZrO_2 is relatively transparent from 4000 to 800 cm^{-1} while SiO_2 is relatively transparent from 4000 to 1400 cm^{-1} and 1000−500 cm^{-1}. The nanopowder-filled grid was mounted into a stage that could be heated to 500 °C. This stage was then loaded into the FTIR reactor such that the IR beam passed through the center of the grid. During in situ FTIR measurements, the substrate temperature was maintained by the heated stage, while the reactor walls were maintained at 200 °C to prevent precursor condensation.

ALD Ga_2O_3 films were deposited onto Si(100) and fused SiO_2 substrates and then characterized by a variety of techniques. The film thickness and optical properties were determined by fixed angle spectroscopic ellipsometry (alpha-SE, J. A. Woollam Co.) using a Cauchy model to fit the ellipsometric data. SEM images were acquired using a Hitachi S4700 with a field-emission electron source and secondary electron detectors. Cross-sectional SEM measurements of cleaved specimens were utilized to confirm the ellipsometric thickness measurements. The morphology and step coverage of the Ga_2O_3 films were assessed by imaging films deposited onto micromachined Si substrates with trenches of varied aspect ratios. The crystallinity of the as-deposited and annealed Ga_2O_3 films was determined by XRD (D8 Advance, Bruker). Annealing to enhance the film crystallinity was conducted in a quartz tube furnace under a flowing UHP Ar atmosphere. The film composition and density were measured by RBS measurements conducted by Evans Analytical Group. The RBS measurements were conducted using a 2.275 MeV He^{2+} ion beam with a backscattering angle of 160° and a grazing angle of 96°. Residual carbon within the Ga_2O_3 film was assessed by XPS spectra acquired by Evans Analytical Group. The film surface was first sputtered with a 4 keV Ar^+ source to remove adventitious carbon and enable sampling of the "bulk" film composition. Optical spectroscopy measurements were performed in transmission mode using a UV−vis-NIR spectrophotometer (Cary 5000, Varian, Inc.). For these measurements, the ALD Ga_2O_3 films were deposited onto both sides of fused SiO_2 substrates, and the measurements were referenced to an uncoated fused SiO_2 substrate.

RESULTS AND DISCUSSION

In situ QCM Measurements. In situ QCM measurements were conducted at reaction temperatures between 250 and 350 °C to evaluate different oxygen sources and processing conditions for Ga_2O_3 ALD. Prior to each experiment, the QCM crystal was first coated with ∼5 nm ALD Al_2O_3 using alternating exposures to TMA and H_2O in order to achieve a reproducible starting surface for the Ga_2O_3 ALD nucleation and growth. In all cases, a mass gain was observed during the first TMGa exposure onto the fresh Al_2O_3 surface, presumably due to the facile chemisorption of the TMGa onto the Al−OH surface hydroxyls. However, sustained mass gains during repeated Ga_2O_3 ALD cycles were only observed with ozone as the oxygen source. Apparently, the H_2O, H_2O_2, isopropanol, O_2, and H_2O/O_2 mixtures are not sufficiently reactive with the TMGa-terminated surface, even at 350 °C. Consequently,

dx.doi.org/10.1021/cm300712x | Chem. Mater. 2012, 24, 4011−4018

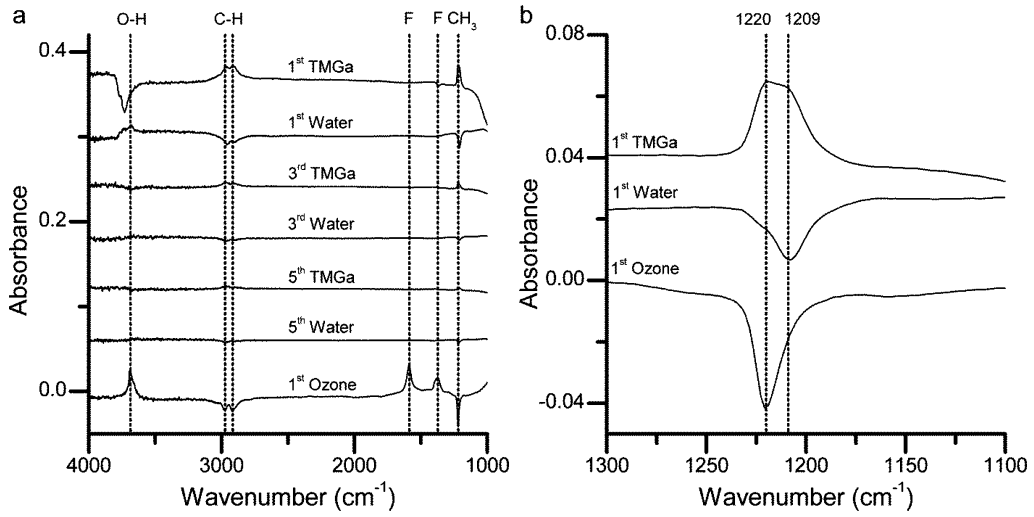

Figure 2. (a) In situ FTIR difference spectra following 1, 3, and 5 TMGa-H_2O exposures and one O_3 exposure at 350 °C. (b) Enlarged image of symmetric CH_3 deformation feature during first TMGa-H_2O cycle and first O_3 exposure. Initial feature due to TMGa adsorption on Al_2O_3 surface consists of peaks at 1209 and 1220 cm^{-1}. H_2O exposure removes only the peak at 1209 cm^{-1}, whereas O_3 exposure removes the peak at 1220 cm^{-1}.

ozone is the only suitable oxygen source for Ga_2O_3 ALD using TMGa. However, an O_2 plasma may work for the plasma-assisted ALD (PEALD) of Ga_2O_3 using TMGa.

Figure 1a shows the mass versus time recorded by QCM during 40 cycles of alternating TMGa-O_3 exposures beginning on an Al_2O_3 surface using the timing sequence 6−10−6−10 at a deposition temperature of 350 °C. The growth is highly linear at 31 ng/cm^2/cycle with no indication of inhibited growth on the initial Al_2O_3 surface. Assuming the β-Ga_2O_3 bulk density of 5.88 g/cm^3, this mass gain corresponds to a growth rate of 0.53 Å/cycle. Figure 1b shows an expanded view of three consecutive Ga_2O_3 ALD cycles. There is an average mass gain of 34.4 ng/cm^2 with each TMGa exposure and a mass loss of 3.4 ng/cm^2 with each ozone exposure, yielding a net mass gain of 31 ng/cm^2 for each complete Ga_2O_3 ALD cycle. These mass changes provide insight into the adsorption of TMGa onto the Ga_2O_3 surface. On the basis of the ligand-exchange mechanism typically observed for metal alkyls on hydroxylated surfaces,[42,43] we propose that the TMGa reacts with OH surface species to lose x CH_3 ligands as CH_4 according to

$$x - \mathrm{OH(s)} + \mathrm{Ga(CH_3)_3(g)} \rightarrow (-\mathrm{O} -)_x\mathrm{Ga(CH_3)_{3-x}(s)} + x\mathrm{CH_4(g)} \quad (1)$$

This mechanism assumes that CH_4 is the only gas phase product formed when TMGa reacts with the surface, which was confirmed by in situ QMS measurements as described below. Using the relationship $R = \Delta m/\Delta m_1$, where Δm is the mass change for one complete cycle and Δm_1 is the mass change upon TMGa adsorption, the amount of CH_3 ligands released, x, can be determined. On the basis of eq 1, Δm = (1/2 Ga_2O_3) = 93.72 and Δm_1 = (Ga) + (3 − x)(CH_3) − x(H) = 114.72−16x. From Figure 1, R = 0.88 and x = 0.51, which implies that fewer than 1 of the 3 CH_3 ligands is released during TMGa adsorption. This relatively small release of CH_3 ligands is consistent with the preferential formation of dimethylgallium species on the surface, as has previously been reported for TMGa adsorption on silica[44] and alumina[45] surfaces.

In situ FTIR Measurements. Both the TMGa-H_2O and TMGa-O_3 processes were characterized using FTIR at a temperature of 350 °C. Prior to the FTIR measurements, the nanopowder-filled grid was allowed to equilibrate at the deposition temperature under flowing UHP N_2 for approximately 1 h and was then passivated with 5 cycles of Al_2O_3 ALD using TMA and H_2O. The FTIR measurements are presented as difference spectra to accentuate the changes resulting from subsequent exposures. A spectrum was recorded after each precursor exposure, and the difference spectrum was generated by subtracting the previous spectrum. Consequently, positive absorbance features indicate the formation of new surface species, whereas negative absorbances indicate the removal of surface species.

The difference spectra over the first five TMGa-H_2O exposures are shown in Figure 2a. With the first TMGa exposure onto the Al_2O_3-coated surface, positive absorbances appear as broad peaks at 2975, 2915, and 1215 cm^{-1}. The 2975 and 2915 cm^{-1} features can be attributed to antisymmetric and symmetric C−H stretching modes, respectively, and the 1215 cm^{-1} feature can be attributed to a symmetric CH_3 deformation mode. The negative absorbance at 3730 cm^{-1} is attributed to the removal of hydroxyl groups. These features are all consistent with previously reported spectra for the adsorption of TMGa onto a hydroxylated Al_2O_3 surface.[45] With the first H_2O exposure, positive absorbances emerge corresponding to the repopulation of hydroxyl groups and negative absorbances appear corresponding to the removal of CH_3 ligands. However, the magnitude of the changes after the first H_2O exposure are smaller than the corresponding changes observed with the first TMGa exposure, suggesting that the CH_3 ligands are only partially removed by H_2O. This pattern continues during subsequent TMGa-H_2O exposures, and by the fifth cycle, practically no absorbance changes were observed. Evidently, successive TMGa-H_2O exposures leave behind CH_3 ligands that eventually passivate the surface and prevent the adsorption of TMGa. This behavior is consistent with our QCM measurements that showed a significant mass gain during the first TMGa exposure onto an Al_2O_3 surface, but progressively smaller mass gains with repeated TMGa-H_2O exposures. These FTIR measurements confirm the finding from QCM that Ga_2O_3 ALD is not possible using alternating TMGa-H_2O exposures.

dx.doi.org/10.1021/cm300712x | Chem. Mater. 2012, 24, 4011−4018

Careful inspection of the CH_3 deformation feature (Figure 2b) reveals some clues regarding the lack of sustained Ga_2O_3 growth with H_2O. The initial CH_3 deformation feature at 1215 cm^{-1} is actually a superposition of two peaks at 1220 and 1209 cm^{-1}. H_2O exposures remove only the peak at 1209 cm^{-1}. As a result, it is the remaining CH_3 groups associated with the 1220 cm^{-1} peak that cause the surface passivation. The exact nature of these two types of CH_3 groups remains unclear. One possibility is that TMGa dissociates on the Al_2O_3 surface to form dimethylgallium species and Al-CH_3 species.[45] As with conventional Al_2O_3 ALD, the Al-CH_3 bonds are easily removed by H_2O, whereas the Ga-CH_3 bonds persist and passivate the surface. Alternatively, in analogy with TMA adsorbed onto an Al_2O_3 surface, the 1220 and 1209 cm^{-1} features may be associated with monomethylgallium and dimethylgallium features, respectively.[46] As with adsorbed TMA, the dimethyl species may be more reactive and removed by the first H_2O exposure, while the monomethyl species are less reactive and remain on the surface. In any case, the persistent peak at 1220 cm^{-1} indicates that surface methyl species prevent Ga_2O_3 ALD using H_2O.

The bottom trace in Figure 2a reveals that after 5 cycles of TMGa-H_2O, a single ozone exposure produced significant absorbance changes. The negative C−H stretching features at 2915 and 2975 cm^{-1} and the negative Ga-CH_3 symmetric deformation feature at 1220 cm^{-1} demonstrate the removal of CH_3 surface groups by ozone. This finding is consistent with our QCM observation that ozone is an effective oxygen source for Ga_2O_3 ALD with TMGa. Additionally, ozone exposure resulted in positive absorbances at 3686 cm^{-1} that correspond to surface hydroxyl groups and at 1586 and 1372 cm^{-1} that correspond to formate groups. These formate groups persist even with ozone exposures of many minutes, indicating their relative stability on the surface. Surface formate groups have also been observed following the ozone exposures for Al_2O_3 ALD using TMA and ozone.[40]

Figure 3 shows difference spectra recorded after successive TMGa and O_3 exposures. The consistent and repeated changes in absorbance associated with the O−H, C−H, formate (F), and CH_3 spectral features signal the exchange of surface functional groups expected for self-limiting surface chemistry. Furthermore, these difference spectra demonstrate that the stable formate groups formed during the ozone exposures are successfully removed during the subsequent TMGa exposures.

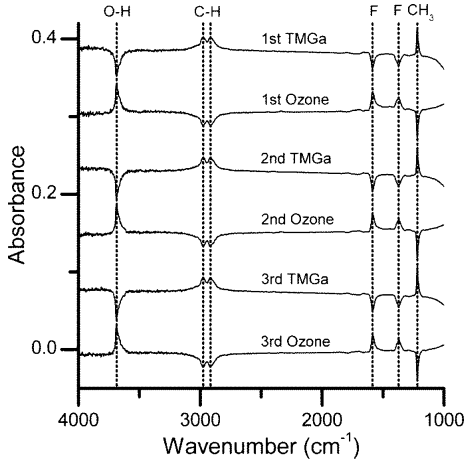

Figure 3. In situ FTIR difference spectra following consecutive TMGa-O_3 exposures at 350 °C.

To verify the net growth of Ga_2O_3 with repeated TMGa-O_3 exposures, we utilized a SiO_2 nanopowder substrate that is transparent in the 800−500 cm^{-1} region, where the bulk Ga_2O_3 modes are expected to appear.[47] Figure 4a shows that the FTIR absorbance (referenced to the initial substrate) in the 800−500 cm^{-1} region increased with increasing Ga_2O_3 ALD cycles, and Figure 4b shows that the integrated absorbance of the Ga_2O_3 bulk modes increased linearly with ALD cycles as expected for layer-by-layer growth.

In situ QMS Measurements. QMS studies were conducted to identify the gaseous products of the TMGa and ozone surface reactions at 350 °C. In these experiments, the TMGa and O_3 precursors were each pulsed twice in succession in order to differentiate the QMS signals resulting from products of the ALD surface reactions from background QMS signals at the same mass to charge (m/e) ratio. We first performed a survey of all m/e values between 10 and 50. On the basis of this survey and the known cracking patterns, we determined that CH_4 (m/e = 15) and CH_2O (formaldehyde, m/e = 29 and 30) were the only significant gaseous products formed during Ga_2O_3 ALD. As shown in Figure 5, CH_4 was the primary product observed during the TMGa exposures, whereas CH_2O was the primary product observed during the ozone exposures. The release of CH_4 is consistent with the dissociative adsorption of TMGa onto the Ga_2O_3 surface and is similar to the CH_4 released during the TMA exposures for Al_2O_3 ALD using TMA and O_3.[40] Consistent with the QCM and FTIR measurements, CH_4 was only observed during TMGa exposures that followed an ozone exposure, because the other oxygen sources left the surface passivated with CH_3 ligands and prevented the adsorption of TMGa and the associated release of CH_4.

The release of CH_2O during the ozone exposures can be explained by the following surface reaction:

$$Ga - CH_3(s) + 2O_3(g) \rightarrow Ga - OH(s) + CH_2O(g) + 2O_2(g) \quad (2)$$

in which O_3 reacts with CH_3 ligands to form surface hydroxyls and CH_2O. We postulate that O_2 is formed in eq 2, but it was not possible to verify this hypothesis by QMS given the enormous background signals from O_2 during the O_3 exposures. The CH_2O shown in eq 2 can desorb and become entrained in the carrier gas flow so that it is sensed by the QMS, or the CH_2O can readsorb onto the Ga_2O_3 to form a surface formate species. This mechanism is consistent with the FTIR results, in that it results in the formation of both hydroxyls and formates. Furthermore, previous FTIR studies have demonstrated the formation of surface formates via the exposure of metal oxides to CH_2O.[40,48,49]

Growth of ALD Ga_2O_3 Films. To evaluate the process conditions for saturated, self-limited growth, we deposited Ga_2O_3 films with varied TMGa and ozone exposure times at both 250 and 350 °C, and the film thicknesses were subsequently measured by ellipsometry. The TMGa saturation was assessed by using the timing sequence of x−5−6−5, whereas the ozone saturation was assessed using the timing sequence of 0.5−5−x−5. As shown in Figure 6a, the Ga_2O_3 growth rate saturated with TMGa exposures as small as 0.5 s. However, the growth rate at 250 °C was ∼20% lower than at 350 °C. Figure 6b shows that the Ga_2O_3 growth rate at 350 °C

dx.doi.org/10.1021/cm300712x | Chem. Mater. 2012, 24, 4011−4018

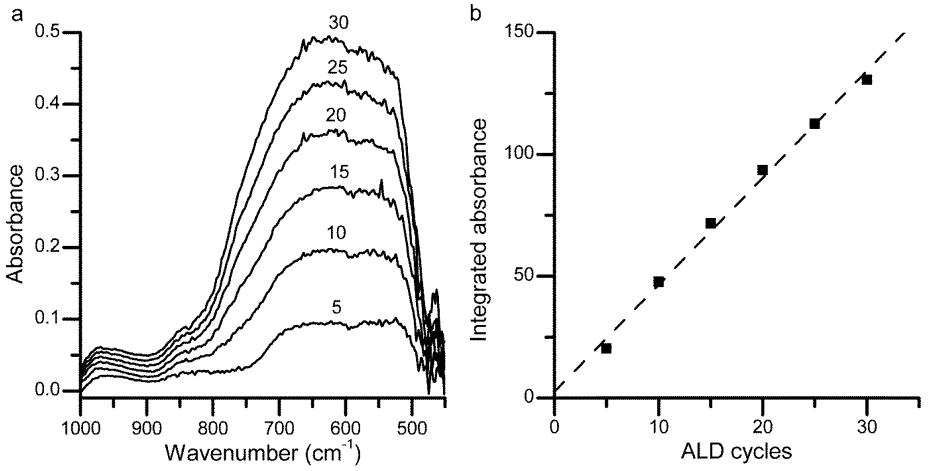

Figure 4. (a) In situ FTIR spectra acquired after 5, 10, 15, 20, 25, and 30 complete TMGa-O_3 ALD cycles at 350 °C referenced to the initial substrate spectrum. (b) Integrated absorbance of spectra in Figure 4a over the range 500−800 cm^{-1} versus the number of TMGa-O_3 ALD cycles.

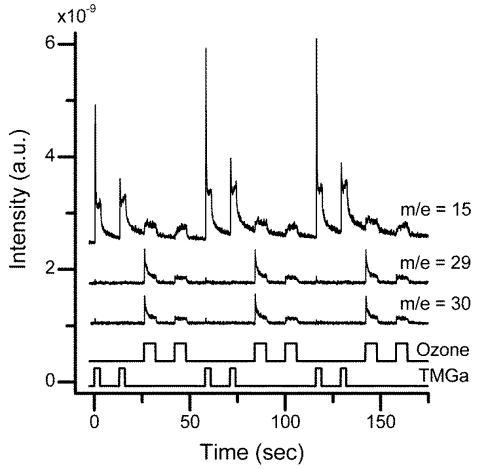

Figure 5. In situ QMS measurements during Ga_2O_3 ALD using TMGa and O_3 where the individual precursor exposures are indicated by the lower traces.

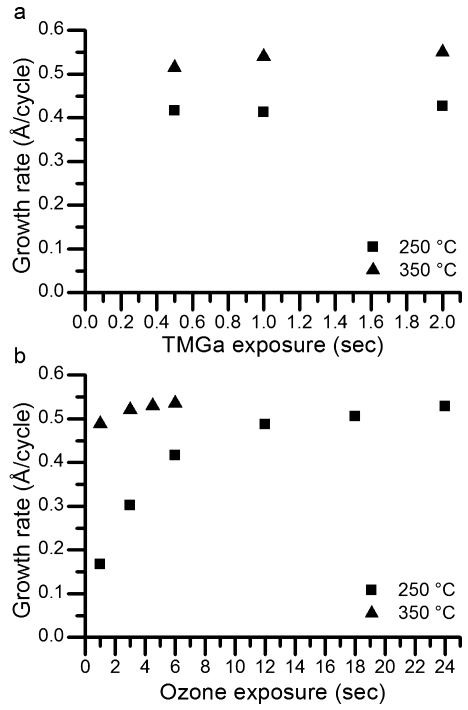

Figure 6. Ga_2O_3 growth rate at 250 and 350 °C as a function of (a) TMGa and (b) O_3 exposures.

saturated at 0.52 Å/cycle using ozone exposure times as short as 3 s, whereas the growth rate at 250 °C required longer ozone exposures of at least 12 s to achieve a saturated growth rate of 0.52 Å/cycle. On the basis of the more rapid ozone saturation achieved at the higher temperature, we believe that the ozone reaction with the TMGa-terminated surface is the rate-limiting step for Ga_2O_3 ALD. Moreover, the lower apparent saturation growth rate at 250 °C in Figure 6a is explained by the subsaturating 6 s ozone exposures used for these measurements.

Figure 7 shows the Ga_2O_3 growth rate as a function of deposition temperature using a fixed TMGa-O_3 timing sequence of 0.5−5−6−5. The Ga_2O_3 growth rate is nearly constant at 0.52 Å/cycle between 300 and 375 °C. The reduced growth rates observed below 300 °C are attributable to the slower ozone reactions, such that 6 s ozone exposures were insufficient to achieve saturation. However, by utilizing much longer ozone exposures, 24 s at 250 °C and 72 s at 200 °C, it was possible to achieve saturated growth at these reduced temperatures. The reduced growth rates above 375 °C may result from the thermal decomposition of the TMGa or ozone precursors upstream of the sample substrates. For example, the onset of reduced growth rate is consistent with the onset of TMGa decomposition that has been previously reported.[50−52] Lastly, the Ga_2O_3 growth rate of 0.52 Å/cycle measured by ellipsometry at 350 °C is very similar to the value of 0.53 Å/cycle determined from the QCM measurements. This close agreement lends confidence to both measurements and indicates that the ALD Ga_2O_3 has a similar density as bulk β-Ga_2O_3.

It is interesting to note that the Ga_2O_3 growth rate of 0.52 Å/cycle is significantly less than the typically observed 1.0−1.2 Å/cycle for TMA-H_2O[27] or 0.8 Å/cycle for TMA-O_3[53] at similar temperatures. Steric hindrance might explain this difference. TMA adsorbs onto ALD Al_2O_3 by losing ∼50% of its CH_3 ligands. In contrast, our QCM measurements demonstrated that TMGa loses only ∼17% of its CH_3 groups upon adsorption onto Ga_2O_3. The steric hindrance imposed by the remaining CH_3 ligands may block the chemisorption of

dx.doi.org/10.1021/cm300712x | Chem. Mater. 2012, 24, 4011−4018

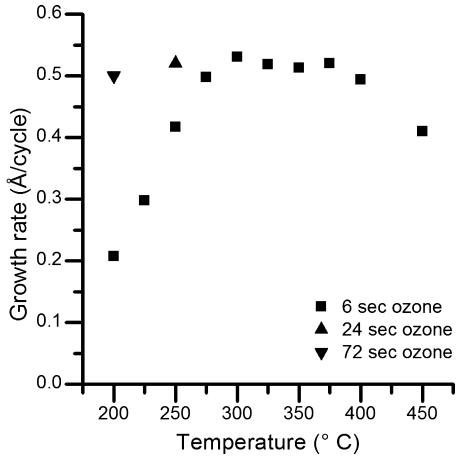

Figure 7. Ga_2O_3 growth rate as a function of the deposition temperature for fixed TMGa exposures of 0.5 s and variable ozone exposures.

additional TMGa and result in a lower Ga_2O_3 growth rate compared to the analogous Al_2O_3 ALD process. Alternatively, the lower growth rate may be attributed to the reduced reactivity of TMGa relative to TMA. Previous studies of TMGa adsorption onto metal oxide surfaces demonstrate reduced reactivity toward bridging oxygen sites compared to TMA.[44] As a result, TMA may have more reactive sites available per cycle (both surface hydroxyls and bridging oxygen sites) and a correspondingly higher growth rate. However, it should be noted that these studies of TMGa adsorption were conducted at 20 °C and not the elevated temperatures being used for ALD, so direct comparison is difficult.

It is also instructive to compare the TMGa-O_3 process with previously reported Ga_2O_3 processes utilizing $Ga(acac)_3$ and $Ga_2(N(CH_3)_2)_6$. The $Ga(acac)_3$ process exhibits a narrow temperature window of 350−375 °C and a growth rate of 0.22 Å/cycle,[19,20] whereas the $Ga_2(N(CH_3)_2)_6$ process exhibits a temperature window of 150−270 °C and a growth rate of 1 Å/cycle.[21−23] At high temperatures, the TMGa process offers clear advantages over the $Ga(acac)_3$ process, with a higher growth rate and larger temperature window. A direct comparison with the $Ga_2(N(CH_3)_2)_6$ process is less clear. Because of their differing temperature windows, these processes can best be considered complementary.

Lastly, the temperature window for Ga_2O_3 ALD is particularly important when considering the deposition of doped or mixed Ga_2O_3 films for applications such as TCOs, phosphors, and GaAs dielectrics. Such deposition requires compatible temperature windows between Ga_2O_3 and dopant ALD processes. For Ga_2O_3, this window is primarily 300−375 °C for reasonable ozone exposure times (≤6 s). However, as demonstrated above, this temperature window can be extended to lower temperatures by using longer ozone exposures.

Properties of ALD Ga_2O_3 Films. To characterize the properties of ALD Ga_2O_3, we deposited films onto Si(100) and fused SiO_2 substrates at 350 °C using a timing sequence of 0.5−5−3−5. The composition of the ALD Ga_2O_3 was evaluated by RBS using a 100 Å Ga_2O_3 film deposited onto Si(100). RBS showed that the films were stoichiometric as-deposited and had the expected Ga:O atomic ratio of 2:3 with no carbon within the 4 at% detection limit for RBS. The density of the ALD Ga_2O_3 was determined by RBS to be 6.31×10^{22} atoms/cm^3. Using the known thickness of 100 Å from ellipsometry, the Ga_2O_3 film density is 5.5 g/cm^3, which is slightly lower than the β-Ga_2O_3 bulk density of 5.88 g/cm^3. As will be demonstrated below, the ALD Ga_2O_3 films are amorphous as-deposited, and this accounts for the lower density. Because of the limited ability of RBS to detect residual carbon within the film, XPS analysis was also conducted. After sputtering into the Ga_2O_3 film, XPS spectra revealed only Ga and O and no detectable carbon within the film. As a result, we conclude that the films are free of residual carbon from the ALD process.

The film morphology and conformality were characterized by SEM using 800 Å thick Ga_2O_3 films deposited onto micromachined Si substrates with trenches 1.2 μm wide and 13 μm deep (aspect ratio = 11). As shown in Figure 8, the Ga_2O_3 films are smooth and featureless, and they coat the entire trench structure. The Ga_2O_3 thickness decreases from 800 Å at the top of the trench to 550 Å at the bottom of the trench. The lower apparent growth rate at the bottom of the trench may result from thermal decomposition of the ozone at these relatively high growth temperatures[54] and would likely improve by using larger ozone exposures. For comparison, Ga_2O_3 films deposited concurrently in trenches 5 μm wide and 17 μm deep (aspect ratio = 1.8) on the same micromachined substrate exhibited perfect conformality.

The phase of the ALD Ga_2O_3 was evaluated using XRD of 800 Å thick Ga_2O_3 films deposited on fused SiO_2. As shown in

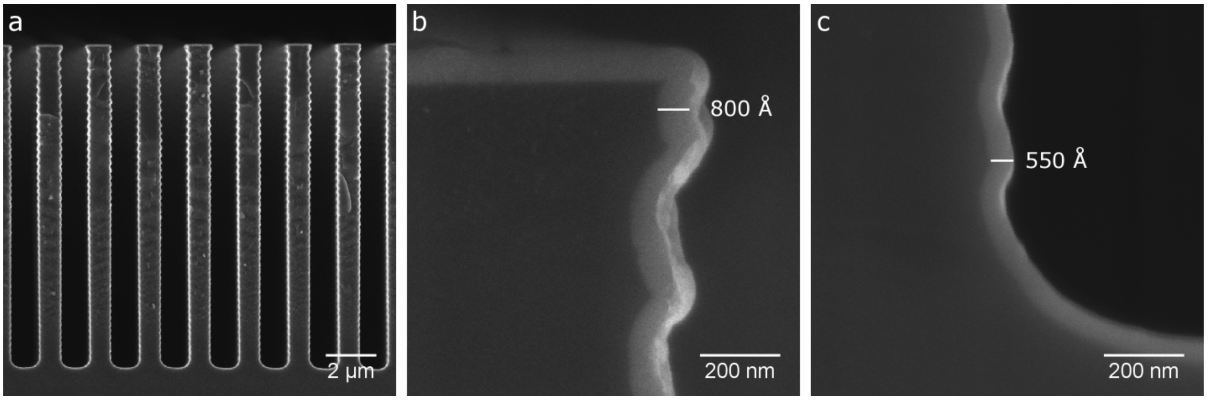

Figure 8. SEM images of 800 Å Ga_2O_3 film deposited onto high-aspect-ratio silicon trenches to assess the conformality of the ALD process: (a) overview of trench structure, (b) top corner of trench with 800 Å Ga_2O_3 thickness, and (c) bottom of trench with 550 Å Ga_2O_3 thickness.

dx.doi.org/10.1021/cm300712x | *Chem. Mater.* 2012, 24, 4011−4018

Figure 9, the as-deposited films were amorphous and exhibited no observable diffraction peaks, which is similar to ALD Ga_2O_3

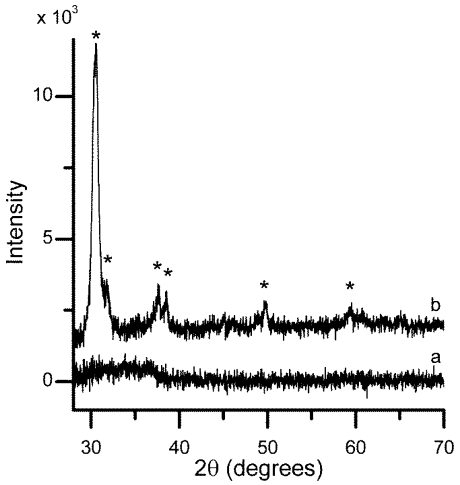

Figure 9. X-ray diffraction data from 800 Å Ga_2O_3 film deposited onto fused SiO_2 with TMGa-O_3 at 350 °C. (a) As-deposited, and (b) after annealing at 900 °C under Ar. Diffraction peaks assigned to β-Ga_2O_3 are indicated by the star symbols.

films prepared using $Ga(acac)_3$[19,20] and $Ga_2(N(CH_3)_2)_6$.[21−23] After annealing at 900 °C for 20 min under Ar, the films exhibited diffraction peaks characteristic of β-Ga_2O_3.

The optical properties of the as-deposited Ga_2O_3 films were determined using ellipsometry and optical transmittance measurements. Fitting the ellipsometric measurements from the ALD Ga_2O_3 films using a Cauchy model provided the refractive index as a function of λ: $n(\lambda) = 1.844 + 0.01249/\lambda^2 + 0.000463/\lambda^4$ with $n = 1.88$ at 589 nm. These refractive index values are very similar to those reported for Ga_2O_3 films prepared by other methods[13,14,55] and to bulk Ga_2O_3.[56] As shown in Figure 10, optical transmittance revealed that the Ga_2O_3 thin films are highly transparent between 300 and 2500 nm. The optical bandgap, E_g, of the Ga_2O_3 film was determined using the relationship $\alpha h\nu = B(h\nu - E_g)^n$, where α is the absorption coefficient as a function hν, B is a constant, and n depends on the type of transition.[57] For these films, the best fit is obtained with $n = 1/2$, which is consistent with a direct bandgap. The E_g is determined by plotting $(\alpha h\nu)^2$ versus energy and extrapolating the linear portion of the curve to zero. As shown in Figure 10b, this analysis reveals a bandgap of 4.95 eV, which is consistent with previous measurements of Ga_2O_3 thin films deposited using other methods and bulk Ga_2O_3.[55] The excellent transmittance and high bandgap of the Ga_2O_3 films makes them well-suited to both TCO and phosphor applications.

CONCLUSIONS

We have demonstrated a new process for the ALD of high-quality Ga_2O_3 thin films using TMGa and ozone. In situ QCM, FTIR, and QMS measurements revealed a growth mechanism in which TMGa dissociatively adsorbs onto the Ga_2O_3 surface to form $Ga(CH_3)_2$ surface species and liberates ~20% of the methyl ligands as CH_4. Next, the ozone reacts with these methyl species to form hydroxyl and formate surface groups and liberate CH_2O. In contrast, Ga_2O_3 ALD using TMGa and H_2O was not possible because the surface became poisoned by surface methyl species after only a few cycles and these methyl

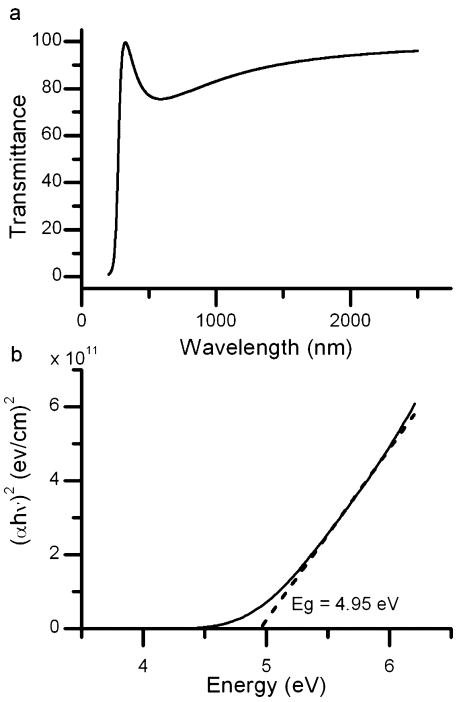

Figure 10. Optical transmittance measurements from 800 Å Ga_2O_3 film deposited onto both sides of a fused SiO_2 substrate. (a) Transmittance of Ga_2O_3 referenced to a fused SiO_2 substrate background, and (b) determination of the optical bandgap of 4.95 eV by fitting the optical absorption data.

species could not be removed by H_2O. Alternating exposures to TMGa and ozone yielded a growth rate of 0.52 Å/cycle for deposition temperatures between 200 and 375 °C. The Ga_2O_3 growth rate decreased at higher temperatures due to precursor thermal decomposition, and larger ozone exposures were required to achieve saturation at temperatures below 300 °C because of the slow ozone kinetics. Analysis of Ga_2O_3 films deposited with the TMGa-O_3 process showed that the films are stoichiometric, free of residual carbon, and possess properties similar to bulk Ga_2O_3. Lastly, the Ga_2O_3 ALD process exhibits a temperature window that is compatible with many complementary ALD processes, which should enable various doped Ga_2O_3 films for applications including TCOs, phosphors, and dielectrics.

AUTHOR INFORMATION

Corresponding Author

*E-mail: jelam@anl.gov.

Notes

The authors declare no competing financial interest.

ACKNOWLEDGMENTS

This work was supported as part of the Center for Electrical Energy Storage: Tailored Interfaces, an Energy Frontier Research Center funded by the U.S. Department of Energy, Office of Science, Office of Basic Energy Sciences. Electron microscopy was performed at the Electron Microscopy Center for Materials Research (EMCMR) at Argonne National Laboratory. Use of the EMCMR was supported by the U.S. Department of Energy, Office of Science, Office of Basic Energy Sciences, under Contract No. DE-AC02-06CH11357 operated by UChicago Argonne, LLC.

REFERENCES

(1) Hao, J. H.; Cocivera, M. *J. Phys. D: Appl. Phys.* **2002**, *35*, 433−438.
(2) Hao, J. H.; Lou, Z. D.; Renaud, I.; Cocivera, M. *Thin Solid Films* **2004**, *467*, 182−185.
(3) Wellenius, P.; Suresh, A.; Muth, J. F. *Appl. Phys. Lett.* **2008**, *92*, 021111.
(4) Podhorodecki, A.; Banski, M.; Misiewicz, J.; Lecerf, C.; Marie, P.; Cardin, J.; Portier, X. *J. Appl. Phys.* **2010**, *108*, 063535.
(5) Orita, M.; Ohta, H.; Hirano, M.; Hosono, H. *Appl. Phys. Lett.* **2000**, *77*, 4166−4168.
(6) Orita, M.; Hiramatsu, H.; Ohta, H.; Hirano, M.; Hosono, H. *Thin Solid Films* **2002**, *411*, 134−139.
(7) Fleischer, M.; Meixner, H. *Sensor. Actuators, B* **1991**, *4*, 437−441.
(8) Ogita, M.; Saika, N.; Nakanishi, Y.; Hatanaka, Y. *Appl. Surf. Sci.* **1999**, *142*, 188−191.
(9) Baban, C.; Toyoda, Y.; Ogita, M. *Thin Solid Films* **2005**, *484*, 369−373.
(10) Hong, M.; Passlack, M.; Mannaerts, J. P.; Kwo, J.; Chu, S. N. G.; Moriya, N.; Hou, S. Y.; Fratello, V. J. *J. Vac. Sci. Technol. B* **1996**, *14*, 2297−2300.
(11) Kwo, J.; Murphy, D. W.; Hong, M.; Opila, R. L.; Mannaerts, J. P.; Sergent, A. M.; Masaitis, R. L. *Appl. Phys. Lett.* **1999**, *75*, 1116−1118.
(12) Paterson, G. W.; Longo, P.; Wilson, J. A.; Craven, A. J.; Long, A. R.; Thayne, I. G.; Passlack, M.; Droopad, R. *J. Appl. Phys.* **2008**, *104*, 103719.
(13) Rebien, M.; Henrion, W.; Hong, M.; Mannaerts, J. P.; Fleischer, M. *Appl. Phys. Lett.* **2002**, *81*, 250−252.
(14) Passlack, M.; Schubert, E. F.; Hobson, W. S.; Hong, M.; Moriya, N.; Chu, S. N. G.; Konstadinidis, K.; Mannaerts, J. P.; Schnoes, M. L.; Zydzik, G. J. *J. Appl. Phys.* **1995**, *77*, 686−693.
(15) Marie, P.; Portier, X.; Cardin, J. *Phys. Status. Solidi A* **2008**, *205*, 1943−1946.
(16) Battiston, G. A.; Gerbasi, R.; Porchia, M.; Bertoncello, R.; Caccavale, F. *Thin Solid Films* **1996**, *279*, 115−118.
(17) Valet, M.; Hoffman, D. M. *Chem. Mater.* **2001**, *13*, 2135−2143.
(18) Binions, R.; Carmalt, C. J.; Parkin, I. P.; Pratt, K. F. E.; Shaw, G. A. *Chem. Mater.* **2004**, *16*, 2489−2493.
(19) Nieminen, M.; Niinisto, L.; Rauhala, E. *J. Mater. Chem.* **1996**, *6*, 27−31.
(20) Nieminen, M.; Lehto, S.; Niinisto, L. *J. Mater. Chem.* **2001**, *11*, 3148−3153.
(21) Shan, F. K.; Liu, G. X.; Lee, W. J.; Lee, G. H.; Kim, I. S.; Shin, B. C. *J. Appl. Phys.* **2005**, *98*, 023504.
(22) Dezelah, C. L.; Niinisto, J.; Arstila, K.; Niinisto, L.; Winter, C. H. *Chem. Mater.* **2006**, *18*, 471−475.
(23) Dezelah, C. L.; Myllymaki, P.; Paivasaari, J.; Arstila, K.; Niinisto, L.; Winter, C. H. *J. Mater. Chem.* **2007**, *17*, 1308−1315.
(24) Lee, H.; Kim, K.; Woo, J. J.; Jun, D. J.; Park, Y.; Kim, Y.; Lee, H. W.; Cho, Y. J.; Cho, H. M. *Chem. Vapor Depos* **2011**, *17*, 191−197.
(25) Putkonen, M. In *Atomic Layer Deposition of Nanostructured Materials*; Pinna, N., Knez, M., Eds.; Wiley-VCH: Weinheim, Germany, 2012; pp 41−51.
(26) Ludowise, M. J. *J. Appl. Phys.* **1985**, *58*, R31−R55.
(27) Puurunen, R. L. *J. Appl. Phys.* **2005**, *97*, 121301.
(28) Kim, H. W.; Kim, N. H. *Mater. Sci. Eng., B* **2004**, *110*, 34−37.
(29) Ott, A. W.; Chang, R. P. H. *Mater. Chem. Phys.* **1999**, *58*, 132−138.
(30) Rahtu, A.; Alaranta, T.; Ritala, M. *Langmuir* **2001**, *17*, 6506−6509.
(31) Elam, J. W.; Groner, M. D.; George, S. M. *Rev. Sci. Instrum.* **2002**, *73*, 2981−2987.
(32) Ferguson, J. D.; Weimer, A. W.; George, S. M. *Thin Solid Films* **2000**, *371*, 95−104.
(33) Ferguson, J. D.; Weimer, A. W.; George, S. M. *Thin Solid Films* **2002**, *413*, 16−25.
(34) Elam, J. W.; Schuisky, M.; Ferguson, J. D.; George, S. M. *Thin Solid Films* **2003**, *436*, 145−156.
(35) Du, Y.; George, S. M. *J. Phys. Chem. C* **2007**, *111*, 8509−8517.
(36) Dameron, A. A.; Seghete, D.; Burton, B. B.; Davidson, S. D.; Cavanagh, A. S.; Bertrand, J. A.; George, S. M. *Chem. Mater.* **2008**, *20*, 3315−3326.
(37) Juppo, M.; Rahtu, A.; Ritala, M.; Leskela, M. *Langmuir* **2000**, *16*, 4034−4039.
(38) Libera, J. A.; Hryn, J. N.; Elam, J. W. *Chem. Mater.* **2011**, *23*, 2150−2158.
(39) Elam, J. W.; Pellin, M. J. *Anal. Chem.* **2005**, *77*, 3531−3535.
(40) Goldstein, D. N.; McCormick, J. A.; George, S. M. *J. Phys. Chem. C* **2008**, *112*, 19530−19539.
(41) Ballinger, T. H.; Wong, J. C. S.; Yates, J. T. *Langmuir* **1992**, *8*, 1676−1678.
(42) Rahtu, A.; Alaranta, T.; Ritala, M. *Langmuir* **2001**, *17*, 6506−6509.
(43) Rahtu, A.; Kukli, K.; Ritala, M. *Chem. Mater.* **2001**, *13*, 817−823.
(44) Morrow, B. A.; McFarlane, R. A. *J. Phys. Chem.* **1986**, *90*, 3192−3197.
(45) McFarlane, R. A.; Morrow, B. A. *J. Phys. Chem.* **1988**, *92*, 5800−5803.
(46) Soto, C.; Wu, R.; Bennett, D. W.; Tysoe, W. T. *Chem. Mater.* **1994**, *6*, 1705−1711.
(47) Escribano, V. S.; Amores, J. M. G.; Lopez, E. F.; Panizza, M.; Resini, C.; Busca, G. *J. Mater. Sci.* **2005**, *40*, 2013−2021.
(48) Busca, G.; Lorenzelli, V. *J. Catal.* **1980**, *66*, 155−161.
(49) Busca, G.; Lamotte, J.; Lavalley, J. C.; Lorenzelli, V. *J. Am. Chem. Soc.* **1987**, *109*, 5197−5202.
(50) Kobayashi, N.; Kobayashi, Y. *Thin Solid Films* **1993**, *225*, 32−39.
(51) Lee, F.; Gow, T. R.; Masel, R. I. *J. Electrochem. Soc.* **1989**, *136*, 2640−2645.
(52) Larsen, C. A.; Buchan, N. I.; Li, S. H.; Stringfellow, G. B. *J. Cryst. Growth* **1990**, *102*, 103−116.
(53) Kim, S. K.; Lee, S. W.; Hwang, C. S.; Min, Y. S.; Won, J. Y.; Jeong, J. *J. Electrochem. Soc.* **2006**, *153*, F69−F76.
(54) Knoops, H. C. M.; Elam, J. W.; Libera, J. A.; Kessels, W. M. M. *Chem. Mater.* **2011**, *23*, 2381−2387.
(55) Al-Kuhaili, M. F.; Durrani, S. M. A.; Khawaja, E. E. *Appl. Phys. Lett.* **2003**, *83*, 4533−4535.
(56) Weast, R. C., Ed. *CRC Handbook of Chemistry and Physics*, 63rd ed.; CRC Press: Boca Raton, FL, 1982.
(57) Pankove, J. I. *Optical Processes in Semiconductors*; Prentice-Hall: Englewood Cliffs, NJ, 1971.